Atmospheric and Climate Sciences, 2025, 15(1), 187-199
https://www.scirp.org/journal/acs
ISSN Online: 2160-0422
ISSN Print: 2160-0414

Multiscale Co-Oscillation Analysis of Solar Radiation and Air Temperature Using Continuous Wavelet Transform: A Case Study of a Tropical Humid Region, Dangbo, Bénin

Ossénatou Mamadou, Djidjoho Renaud Roméo Koukoui, David Gnonlonfoun

Institut de Mathématiques et de Sciences Physiques, Université d'Abomey-Calavi, Dangbo, Bénin
Email: ossenatou.mamadou@imsp-uac.org

How to cite this paper: Mamadou, O., Koukoui, D.R.R. and Gnonlonfoun, D. (2025) Multiscale Co-Oscillation Analysis of Solar Radiation and Air Temperature Using Continuous Wavelet Transform: A Case Study of a Tropical Humid Region, Dangbo, Bénin. *Atmospheric and Climate Sciences*, **15**, 187-199.
https://doi.org/10.4236/acs.2025.151009

Received: November 23, 2024
Accepted: January 13, 2025
Published: January 16, 2025

Abstract

The use of solar energy is today widely recognized for the green transition but also for addressing societal challenges associated with the rise in global surface temperature. The design of a photovoltaic solar panel field may require an understanding of how solar radiation oscillates with other variables or factors since multiple interactions occur during its transfer within the atmosphere. In this study, three years of the incoming shortwave radiation (SWin) and air temperature (Tair) data acquired within the "Institut de Mathématiques et de Sciences Physiques" were analyzed using the continuous wavelet transform to extract the inherent variability of these signals. The underlying characteristics meaning the timescale of these variabilities as well as the lead-lag relationship between SWin and Tair were also examined. With the wavelet power spectrum, the highest variability was evidenced at the 2 - 8 band period for the SWin, coinciding almost with that of Tair. This suggests that these two signals are well interconnected at this temporal scale. The results obtained with the phase ($\varnothing_{xy}$) difference analysis, reveal that SWin leads Tair by ~ 23.5˚ on average when ($0 < \varnothing_{xy} < \pi/2$) whereas when ($-\pi/2 < \varnothing_{xy} < 0$), Tair leads SWin. They demonstrate at least that at the short time scale (*i.e.*, periods ≤ 32 days), Tair increases with an increasing SWin since the lags between these two signals range between 0.09 - 2.30 days. However, when looking at their interdependence at a larger temporal scale (> 32 days), Tair lags SWin. An increase in SWin might not directly imply an increase in Tair. Overall, these findings give insight into complex relationships across scales between the incoming shortwave radiation and air temperature in a tropical humid region of Bénin.

Keywords

Solar Radiation, Air Temperature, Co-Oscillation, Wavelet Transform, Humid Climate, West Africa

1. Introduction

The use of solar energy is today undeniable not only for the green transition but also for addressing societal challenges associated with the rise in global surface temperature. The deployment of this environmentally-friendly form of renewable energy allows fulfilling a number of Sustainable Development Goals (SDGs) while lowering atmospheric greenhouse gas emissions [1] [2], reducing air pollution [3]-[5], and as well as already demonstrated worldwide, supporting energy self-sufficiency [6] [7] and economic development [8]-[10]. Indeed, solar rays are composed of different wavelengths, and the most targeted for photovoltaic solar resources, passive solar design and solar-thermal systems [11] are those coming from the visible and near infrared domains where the maximum energy is expected [12]. However, several factors affect this natural resource during its transfer within the atmosphere. The incident shortwave radiation emitted by the sun, for example, undergoes several processes of diffusion, reflection and transmission by the atmospheric particles which lower its amount before it reaches the ground [12]. Thus, the amount of radiation arriving at the surface depends mainly on the state, characteristics of the atmosphere, topography of the surface etc. Thereby, it remains crucial in the design of operational solar energy projects, performance assessment or preferably before installing a solar firm at a site for example, to conduct an experimental campaign and analyze the acquired data to extract information on the variability of this natural resource. A campaign will be useful to extract the inherent variability of the resource and far away to understand its underlying characteristics meaning the timescale at which interactions between solar radiation and atmospheric particles occur for a region of interest. This also could be of great importance for modelling studies [11] [13]-[15] especially in regions where meteorological observations and dedicated solar radiation measurements are scarce.

Because of the lack of in situ measurements, many solar radiation models have been developed using several methods based on meteorological data and including among others, sunshine duration, relative humidity, cloud cover, minimum and maximum air temperature. With regard to this, their study done in Madrid [11] [16] showed that the model based on temperature provides better results if its parameters are correctly adjusted. Indeed, these authors developed a new empirical model using the theoretical maximum possible value of radiation through daily maximum and minimum air temperature to estimate global solar radiation on a daily scale in Madrid. [17] exploited the inter-relationship between daily atmospheric transmission coefficients, air temperature and sunshine duration to estimate solar radiation in various sites worldwide. In a tropical region of West Africa, [18] clearly emphasizes the importance of the maximum air temperature in solar radiation modelling in Nigeria. These authors showed that maximum air temperature and relative humidity can be used together to predict solar radiation with satisfactory accuracy. [19] proposed a simple model for determining solar radiation from extraterrestrial radiation and the measured temperature range. [20] assumed that solar radiation should be an exponential function of temperature difference at a daily time scale. In all these modelling studies, air temperature appears as a key variable, from which one can estimate or predict solar radiation due to the strong relationship between these two variables. Since the air temperature is the most common and available meteorological variable, understanding this relationship in a unified time-frequency scale could be therefore an interesting mean or a prerequisite to understanding firstly the microclimate of this area but can be used to provide relevant knowledge for predicting and modelling radiation processes for a given region.

Recently [21] has shown that there is a lag between SWin and Tair across seven sites spanning from a wetter climate in southern Benin to drier in Mali, West Africa. In northern Benin in particular, characterized by a Sudanian climate (~1200 mm/y), these authors found that the air temperature leads the incoming shortwave radiation meaning that there is a delay in the atmospheric column heating which begins at the ground as suggested by [22]. However, the south of Benin is more humid (sub-equatorial climate with a relative humidity always higher than 50% all year long) [23] compared to the north. We thus hypothesize that surface processes or mechanisms leading or lagging them could be different. Let's recall that there is a lack of research with regard to how these preceding processes occur specifically in the south of Benin as highlighted recently by [24]. A solid understanding of the physical processes combined with the data of specific variables that represent them is a necessary first step from which forecasters may be able to provide better predictions about solar radiation availability and enable early actions.

The objective of this study is therefore to analyze the co-oxillation between the SWin and Tair in both time and frequency domains. This relationship is examined utilizing the Continuous Wavelet Transform (CWT) framework, enabling to distinguish during the analyzed years both interconnections in time as well as short- and long term connections. The analysis is applied to the data acquired at the southeastern part of Bénin using daily average data spanning from November 2020 to October 2023. We also provide annual cycles to emphasize the radiative characteristics of this area. In the remainder of this paper, the site and data used are presented in Section 2; different methodological approaches are described in Section 3. The temporal dynamics of SWin and Tair at seasonal timescale are presented in Section 4 .1. We then highlight the findings obtained using the spectral method in Sections 4.2 and 4.3, followed by a discussion. Finally, conclusions are drawn in Section 5.

2. Site and Data Acquisition

The measurements of the air temperature and incoming shortwave radiation were conducted at the Dangbo Eddy Covariance (EC) site established in the "Institut de Mathématiques et de Sciences Physiques", southeast Bénin (Figure 1). The observational station was set up in October 2020 within the framework of the ASEEW@ research project [23], funded by the OWSD Early Career Fellowship, and is currently part of the "DangboFLUX" initiative. In this study, we used meteorological data spanning from November 2020 to October 2023 thus three complete years to investigate the co-oscillation in the spectral domain of the air temperature and incoming shortwave radiation. The studied region is characterized by a typical subequatorial climate with two rainy seasons alternating with long and short dry seasons [23] [25]. Air temperature measurements were acquired utilizing an EE181 probe while the incoming shortwave radiation data were obtained using a CNR4 Net radiometer. Data were recorded each 15 min and stored continuously in the datalogger.

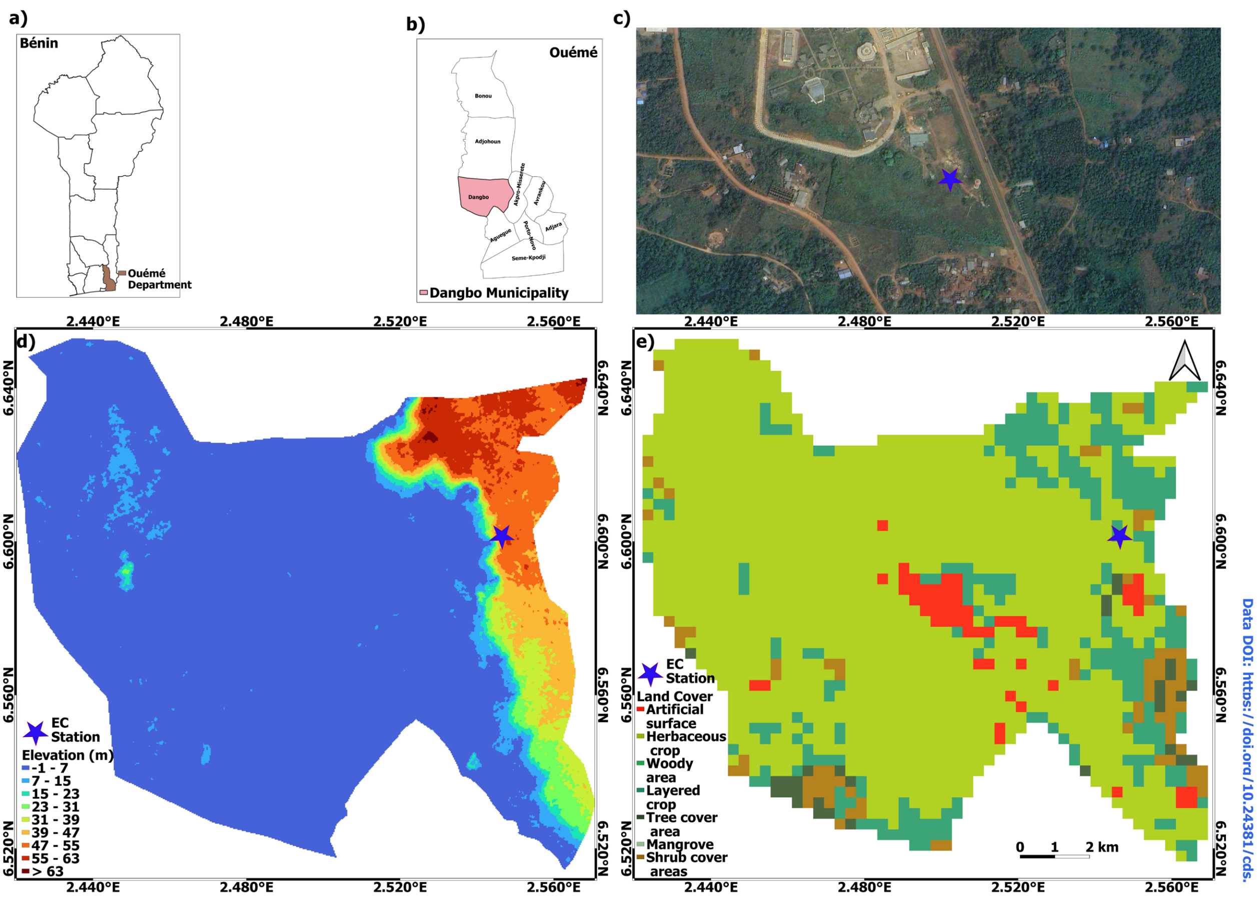

Figure 1. Location of (a) Ouémé in Bénin, (b) the Dangbo municipality in the Ouémé department; (c) google earth view of the study area. The star indicates the location of the study site. (d) altitude of the area and (f) land cover in the Dangbo municipality from [23].

3. Wavelet Transform Analysis

Data acquired with these sensors were used to investigate changes in solar radiation, and in air temperature as well their lead-lag relationship using the wavelet transforms since they are suitable to analyzing non-stationary processes [26]. The wavelet analysis is a transformation of time and frequency which is used to extract relevant information from a signal or a sequence of observation and analyze it at multiscale through dilatation and translation [27] [28]. It decomposes the variance of signal into series of coefficients which represents the distribution of the variance across different frequencies (scales) and time (location) [26] [29]. It is able to highlight, as a spectral method, a specific behavior in the signals and therefore useful to understanding time-frequency variation of the two signals as well revealing their singularities. The Wavelet Transform of a signal $x(t)$ noted $WT_x(\tau, s)$ for a given scale "s" is defined as:

$$WT_x(\tau, s) = \beta * \sum_{t=1}^{N} x \frac{1}{\sqrt{s}} \psi^* \left(\frac{(t-\tau)\delta t}{s} \right), \tag{1}$$

where τ is the translation parameter indicating of the position of the wavelet; δt is the temporal scale; $\beta = (\delta t / s)^{1/2}$ is the normalization factor necessary to ensure the variance unity of the wavelet coefficients; ψ^* is the conjugate of the mother function satisfying the wavelet admissibility criterion. In this work, the commonly complex mother function widely used in atmospheric time series analysis, that is the Morlet mother function, has been chosen because of its complex form given by:

$$\psi(t) = \pi^{-\frac{1}{4}} e^{iwt} e^{-\frac{t^2}{2}}. \tag{2}$$

By dilating (or contracting) the scale (s) and translating within time (τ), one can calculate the wavelet coefficients ($WT_x(\tau, s)$), which characterize how different scales (s) contribute to the time series x_t at various time positions (τ). The wavelet power spectrum WPS_x which represents indeed the variance of the signal $x(t)$ is computed from $WT_x(\tau, s)$ as:

$$WPS_x(\tau, s) = 2^s \left| WT_x(\tau, s) \right|^2. \tag{3}$$

WPS gives the local repartition of the energy in time and describes how much each period or frequency band contributed to the energy of the signal over that time interval. The higher the WPS is, the larger is the variance of the signal and vice versa.

3.1. Wavelet Coherence

The wavelet coherence of two signals $x(t)$ and $y(t)$, analogous to the correlation in a standard statistical analysis, is used to explore the localized linear relationship between incoming shortwave radiation and air temperature at different scales (frequencies) over the time. It is expressed as:

$$R_{xy}^2(s) = \frac{\left| \left\langle s^{-1} WT_{xy}(\tau, s) \right\rangle \right|^2}{\left\langle s^{-1} \left| WT_x(\tau, s) \right|^2 \right\rangle \left\langle s^{-1} \left| WTy(\tau, s) \right|^2 \right\rangle}, \tag{4}$$

where $\langle \cdots \rangle$ in Equation (4) is the time and frequency smoothing operator for the Morlet wavelet. $WT_{xy}(\tau, s)$ the cross-wavelet transform of $x(t)$ and $y(t)$ given by:

$$WT_{xy}(\tau, s) = WT_x(\tau, s) WT_y^*(\tau, s), \quad (5)$$

where $WT_y^*(\tau, s)$ is the complex conjugate of $WT_y(\tau, s)$.

R_{xy}^2 ranges from 0 to 1; the larger the value, the higher the coherence means greater linear correlation between variables. By transforming incoming shortwave radiation and air temperature data into scales via Equations (1)-(3), the amplitude spectra provides clear spatial variability while the phase indicates their discontinuities.

3.2. Phase Difference

The cross-wavelet transform also provides the lead and lag relationship in oscillations between two time series. They are known as a phase difference [27] and can be used to extract information about the nature of correlation processes between signals under the assumption that they are causal [30]. The phase difference $\varnothing_{xy}$ is given by:

$$\varnothing_{xy} = \tan^{-1}\left(\frac{\mathrm{Re}\left(W_{xy}(\tau, s)\right)}{\mathrm{Im}\left(W_{xy}(\tau, s)\right)}\right). \quad (6)$$

where $\varnothing_{xy}$ represents phase difference varying in the interval [−π; π]; $\mathrm{Re}\left(W_{xy}(\tau, s)\right)$ and $\mathrm{Im}\left(W_{xy}(\tau, s)\right)$ are the real and imaginary parts of $W_{xy}(\tau, s)$. When $\varnothing_{xy}$ ∈ [0, π/2], x, y move in phase meaning they are positively correlated and x leads y; $\varnothing_{xy}$ ∈]−π/2, 0], x, y move in phase and y leads x. If $\varnothing_{xy}$ ∈] π/2; π], the two time series are negatively correlated (anti-phase) and x is out of phase and leads y and finally for the last quadrant y is out of phase and leads x.

4. Results and Discussion

4.1. Thermal Conditions

Figure 2 shows the three-year time series data of the incoming shortwave radiation (SWin) and air temperature (Tair), respectively, observed at Dangbo from 01 November 2020 (01 November corresponds to Day of Year (DOY) 1) to 31 October 2023 (DOY 365).

The solar radiation (SWin) reaching the ground at Dangbo exhibited a certain variability which is more pronounced during the wet season (from March to June and September to October). Its evolution also showed a sizeable influence of cloudiness and other factors, limiting the amount of radiation arriving at the surface. In addition, the pattern of SWin reveals the presence of nonlinearities and multiple time scales of variations, which are higher in wet seasons (March to June and September to October) and lower in dry seasons (July to August and November to February respectively).

The distinct SWin and Tair annual patterns in the studied area illustrated in Figure 2 are pieces of evidence that contrast the three years studied but also within the annual cycle. The annual daily average air temperature was about 26.8˚C ± 1.4˚C and the incoming shortwave radiation was 180 ± 50 $W \cdot m^{-2}$ (mean ± s.d.) over the studied period.

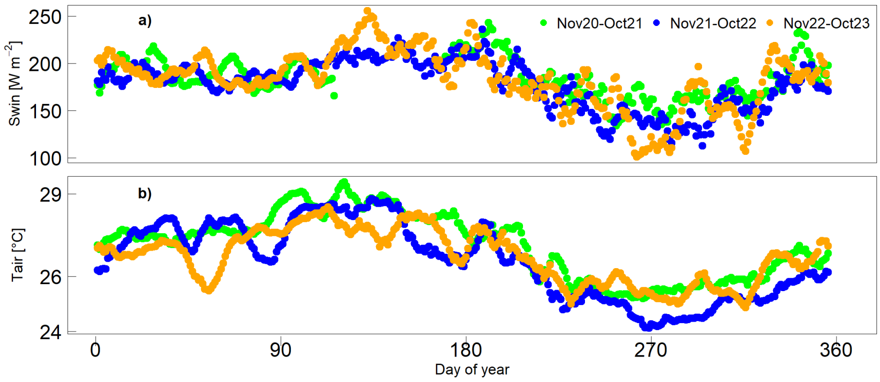

Figure 2. Daily average of: (a) the incoming shortwave radiation and (b) air temperature for the three years analyzed: November 2020 to October 2021 (green); November 2021 to October 2022 (blue) and November 2022 to October 2023 (orange). Day of year (DOY) represents the number of day within the year.

On average, SWin increases from DOY 100 (around January) to reach its first maxima around DOY 150 (March) but then weakens slowly until July/August where the annual minimum value is observed. The following increase is sharp and lasts until the end of the year (October 31st). The annual evolution of Tair follows a little that of SWin. It is interesting to note that the daily maximum is roughly the same during the three years (~29.0˚C - 30.0˚C), occurring between DOY 100 (during the long dry season) and DOY 150 (March) at the beginning of the wet season. The minimum values (~24.0˚C - 25.0˚C) were however found, depending the year in July/August/September which coincides with the high cloudiness period in West Africa [31]-[33].

4.2. Continuous Wavelet Transform Analysis of SWin and Tair

Figure 3 presents the daily wavelet power spectrum of the incoming shortwave radiation (SWin) and air temperature (Tair) at the Dangbo site. Herein, we quantified the variability of these signals with the wavelet coefficient at different time scales and periods. Two major peaks of variability (2 - 8 and 64 - 128 bands) were emphasized with the wavelet power spectrum (WPS) of SWin. The highest value of the WPS was obtained within the 2 - 8 band period and was more concentrated suggesting that there is a higher variance in the signal from daily to almost decadal time period. The second peak is less higher, with some abrupt and localized changes in the variance of SWin revealing rather the difference between months (thus seasons) corresponding to the seasonal variability of SWin. This evidences also the presence of nonlinearities at these scales already emphasized in previous section (**Figure 2**). When looking at **Figure 3**, annual pattern of SWin is clearly depicted with higher power during wet seasons (March to June and September to October) and slight to almost inexistent power during dry season especially between January and February and within the 2 - 8 band period.

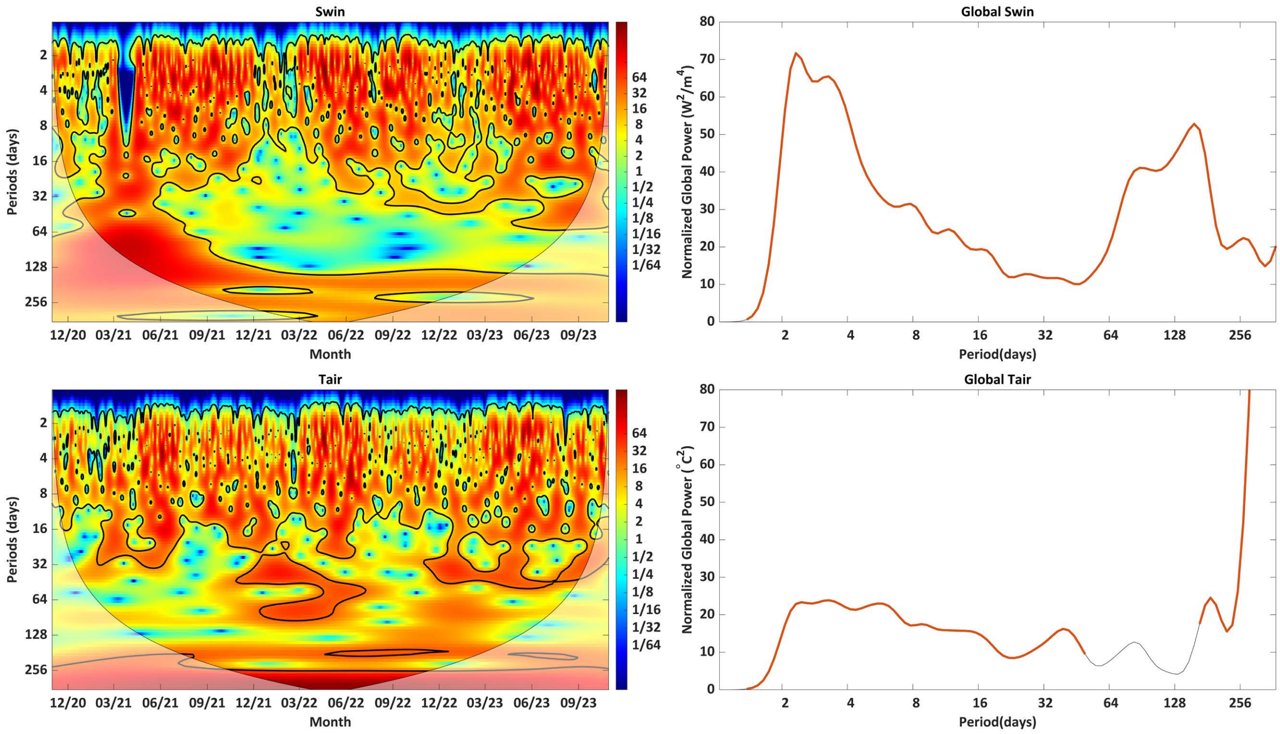

Figure 3. Continuous wavelet transform of the daily incoming shortwave radiation (SWin) and air temperature (Tair) (left) and their respective global spectra (right) according to the period from November 2020 to October 2023. Areas of statistical significance are circled in black; the area outside the cone of influence has no statistical significance.

The highest wavelet power in SWin coincides almost with that of Tair indicating that these two variables are interconnected especially in the 2 - 8 band period. Beyond this band, there is relatively continuous and lower power of variability compared to the 2 - 8 band. Wavelet coefficients acutely vary form the highest to the lowest suggesting a potential unstable variability of Tair between 16 and 256 band period.

4.3. Coherence and Lead-Lag Analyses

In respect of each band of time, and period, color gradation indicates the level of co-oscillation (weak or strong). The arrow directions indicate however the causation (leading of lagging) and the nature of the relationship. The degree of co-oscillation was reflected through the plots in the time frequency domain. The color ranged from light blue to red, each representing low and high degree of correlation. The red region indicates a stronger co-oscillation while the blue area indicated a weaker co-oscillation. We can see from (**Figure 4**) that there is a significant co-movement as expected between SWin and Tair across frequencies (periods).

There are some irregular and discontinuous high and low power oscillations for the period below 4 days. For the three years investigated, there is a quasi-inexistence of significant correlation between SWin and Tair during the long dry season for the period lower than 8 days suggesting that there is another possible mechanism that happens at this site and at daily time scale. [23] showed for example that at this site, a lower RH is not accompanied by a high air temperature at daily time scale, suggesting that air mass has changed, a drier air mass with the same temperature has arrived over the site. During other periods of the year, both signals depicted some similarity toward a large significant band of variability, sometimes discontinuous, and mostly positive correlation in 2022 and 2023. Based on the daily data analyzed, we found that SWin and Tair move in phase meaning there are positively correlated (arrows directed to the right on the Figure 4), except between December 2022 and February 2023 (long dry season), where arrows are oriented into the left suggesting rather a negative correlation. A clear distinction of the nature of co-oscillation during the long dry season is therefore obtained.

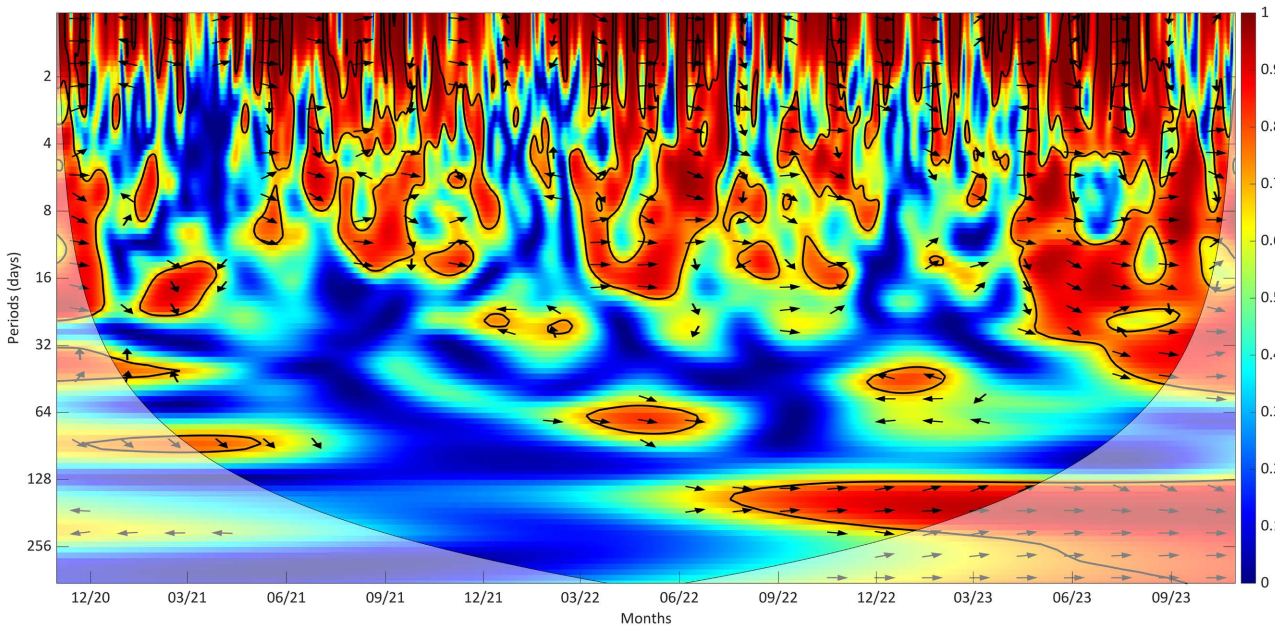

Figure 4. Wavelet coherence between the daily average of SWin and Tair time series spanning from November 2020 to October 2023. Areas of statistical significance are circled in black; the area outside the cone of influence has no statistical significance.

The mean values of coherence (R^2_{xy}), phase ($\varnothing_{xy}$) (where x refers to SWin and y to Tair) and time lags per band period and for the all three years are given in (Table 1) to quantify nature of the co-oscillation within this unified time-frequency domain. On average for the all band periods, $0 < \varnothing_{xy} < \pi/2$, except within the 32 - 64 and 128 - 256 band period where $\varnothing_{xy}$ equaled to 333.84˚ and 347˚ respectively. The former indicates that SWin leads Tair by ~23.5˚ when ($0 < \varnothing_{xy} < \pi/2$) whereas when ($-\pi/2 < \varnothing_{xy} < 0$), Tair leads SWin.

These results suggest at least that at the short time scale (*i.e.* periods ≤ 32 days), Tair increases with an increasing SWin. The lag of these two signals ranges between

0.09 and 2.30 days thus suggesting that the air column heats up almost instantaneously as radiation increases. However, when looking at the interdependence of radiation and air temperature at a larger temporal scale (>32 days), Tair lags SWin meaning that an increase in SWin may not directly imply an increasing Tair. The lags between SWin and Tair within 32 - 64 and 128 - 256 band period are negative and were −3.37 and −6.26 days respectively. Surprisingly, in the 64-128 band period, (R_{xy}^2) was the smallest (0.76) and $\varnothing_{xy}$ = 30 with a lag of 7.72 days between SWin and Tair. This suggests that Tair follows the dynamics of SWin but with a higher delay compared to that of the period ≤ 32 days. All these results together reveals complex dynamics of radiation and air temperature within the annual cycle.

Table 1. The estimates per periods of the local coherence (R_{xy}^2) and the lead-lag relationship ($\varnothing_{xy}$) for the incoming shortwave radiation and air temperature based on the phase angle difference of the wavelet coherence.

Periods (days)	R_{xy}^2	$\varnothing_{xy}$	Lags (days)
2 - 4	0.85	12.07	0.09
4 - 8	0.82	21.71	0.34
8 - 16	0.81	20.03	0.64
16 - 32	0.82	35.76	2.30
32 - 64	0.78	333.84	−3.36
64 - 128	0.76	30.0	7.72
128 - 256	0.83	347	−6.26

5. Conclusion

The data acquired at Dangbo in the years 2020-2023 made it possible to investigate the spectral behavior of the incoming shortwave radiation and air temperature and how these signals vary with respect to time. The SWin and Tair patterns were found to depend considerably on atmospheric state, and on cloudiness in particular. It was possible to determine within a unified time interval-frequency band space where the relationship was present (absent), strong (weak) and positive (negative) and as well as the lag between the two signals involved in the analysis. In addition to the scientific interest, the results obtained in this work may benefit engineers and practicians, as well as those who are interested in knowing how far this natural resource is affected by weather characteristics in the southeastern region of Benin. In a country where energy availability is of critical relevance, the availability of useful and usable weather information is paramount to support its industry and socioeconomic growth.

Author Contributions

OM conceived, designed and wrote the manuscript. All authors discussed the content of the manuscript.

Conflicts of Interest

The authors declare no conflicts of interest regarding the publication of this paper.

References

[1] Jayachandran, M., Gatla, R.K., Rao, K.P., Rao, G.S., Mohammed, S., Milyani, A.H., *et al.* (2022) Challenges in Achieving Sustainable Development Goal 7: Affordable and Clean Energy in Light of Nascent Technologies. *Sustainable Energy Technologies and Assessments*, **53**, Article 102692. https://doi.org/10.1016/j.seta.2022.102692

[2] Maka, A.O.M. and Alabid, J.M. (2022) Solar Energy Technology and Its Roles in Sustainable Development. *Clean Energy*, **6**, 476-483. https://doi.org/10.1093/ce/zkac023

[3] Bergin, M.H., Ghoroi, C., Dixit, D., Schauer, J.J. and Shindell, D.T. (2017) Large Reductions in Solar Energy Production Due to Dust and Particulate Air Pollution. *Environmental Science & Technology Letters*, **4**, 339-344. https://doi.org/10.1021/acs.estlett.7b00197

[4] Boudri, J.C., Hordijk, L., Kroeze, C., Amann, M., Cofala, J., Bertok, I., *et al.* (2002) The Potential Contribution of Renewable Energy in Air Pollution Abatement in China and India. *Energy Policy*, **30**, 409-424. https://doi.org/10.1016/s0301-4215(01)00107-0

[5] Shahsavari, A. and Akbari, M. (2018) Potential of Solar Energy in Developing Countries for Reducing Energy-Related Emissions. *Renewable and Sustainable Energy Reviews*, **90**, 275-291. https://doi.org/10.1016/j.rser.2018.03.065

[6] Kabeyi, M.J.B. and Olanrewaju, O.A. (2022) Sustainable Energy Transition for Renewable and Low Carbon Grid Electricity Generation and Supply. *Frontiers in Energy Research*, **9**, Article 743114. https://doi.org/10.3389/fenrg.2021.743114

[7] Kondi-Akara, G., Hingray, B., Francois, B. and Diedhiou, A. (2023) Recent Trends in Urban Electricity Consumption for Cooling in West and Central African Countries. *Energy*, **276**, Article 127597. https://doi.org/10.1016/j.energy.2023.127597

[8] Anam, M.Z., Bari, A.B.M.M., Paul, S.K., Ali, S.M. and Kabir, G. (2022) Modelling the Drivers of Solar Energy Development in an Emerging Economy: Implications for Sustainable Development Goals. *Resources, Conservation & Recycling Advances*, **13**, Article 200068. https://doi.org/10.1016/j.rcradv.2022.200068

[9] Timilsina, G.R., Kurdgelashvili, L. and Narbel, P.A. (2012) Solar Energy: Markets, Economics and Policies. *Renewable and Sustainable Energy Reviews*, **16**, 449-465. https://doi.org/10.1016/j.rser.2011.08.009

[10] Zhao, L., Wang, W., Zhu, L., Liu, Y. and Dubios, A. (2018) Economic Analysis of Solar Energy Development in North Africa. *Global Energy Interconnection*, **1**, 53-62. https://doi.org/10.14171/j.2096-5117.gei.2018.01.007

[11] Almorox, J., Hontoria, C. and Benito, M. (2011) Models for Obtaining Daily Global Solar Radiation with Measured Air Temperature Data in Madrid (Spain). *Applied Energy*, **88**, 1703-1709. https://doi.org/10.1016/j.apenergy.2010.11.003

[12] Iqbal, M. (1983) Ground ALBEDO. In: IQBAL, M., Ed., *An Introduction to Solar Radiation*, Elsevier, 281-293. https://doi.org/10.1016/b978-0-12-373750-2.50014-8

[13] Hassan, G.E., Youssef, M.E., Mohamed, Z.E., Ali, M.A. and Hanafy, A.A. (2016) New Temperature-Based Models for Predicting Global Solar Radiation. *Applied Energy*, **179**, 437-450. https://doi.org/10.1016/j.apenergy.2016.07.006

[14] Prieto, J.I., Martínez-García, J.C. and García, D. (2009) Correlation between Global Solar Irradiation and Air Temperature in Asturias, Spain. *Solar Energy*, **83**, 1076-1085. https://doi.org/10.1016/j.solener.2009.01.012

[15] Wong, L.T. and Chow, W.K. (2001) Solar Radiation Model. *Applied Energy*, **69**, 191-224. https://doi.org/10.1016/s0306-2619(01)00012-5

[16] Almorox, J. (2011) Estimating Global Solar Radiation from Common Meteorological Data in Aranjuez, Spain. *Turkish Journal of Physics*, **35**, 53-64. https://doi.org/10.3906/fiz-0912-20

[17] Abraha, M.G. and Savage, M.J. (2008) Comparison of Estimates of Daily Solar Radiation from Air Temperature Range for Application in Crop Simulations. *Agricultural and Forest Meteorology*, **148**, 401-416. https://doi.org/10.1016/j.agrformet.2007.10.001

[18] Ododo, J.C., Sulaiman, A.T., Aidan, J., Yuguda, M.M. and Ogbu, F.A. (1995) The Importance of Maximum Air Temperature in the Parameterisation of Solar Radiation in Nigeria. *Renewable Energy*, **6**, 751-763. https://doi.org/10.1016/0960-1481(94)00097-p

[19] Hargreaves, G.H. and Samani, Z.A. (1982) Estimating Potential Evapotranspiration. *Journal of the Irrigation and Drainage Division*, **108**, 225-230. https://doi.org/10.1061/jrcea4.0001390

[20] Bristow, K.L. and Campbell, G.S. (1984) On the Relationship between Incoming Solar Radiation and Daily Maximum and Minimum Temperature. *Agricultural and Forest Meteorology*, **31**, 159-166. https://doi.org/10.1016/0168-1923(84)90017-0

[21] Davies, P., Mamadou, O., Quansah, E., Aryee, J.N.A., Atiah, W.A., Amekudzi, L.K., *et al.* (2022) Variability in Surface Radiative Fluxes over West Africa Using Wavelet and Principal Component Analyses. *GSA Research Seminar and Poster Presentations*, KNUST Kumasi, 7-8 June 2022, 141.

[22] Garratt, J.R. (2001) Clear-Sky Longwave Irradiance at the Earth's Surface—Evaluation of Climate Models. *Journal of Climate*, **14**, 1647-1670. https://doi.org/10.1175/1520-0442(2001)014<1647:csliat>2.0.co;2

[23] Mamadou, O., Mariscal, A., Koukoui, D.R.R., Hounsinou, M. and Kounouhéwa, B. (2024) Meteorological Conditions and Second-Order Moments of Wind Speed Components over a Nonuniform Terrain in Dangbo, Southeastern Benin. *Meteorology and Atmospheric Physics*, **136**, Article No. 47. https://doi.org/10.1007/s00703-024-01043-x

[24] Bodjrenou, R., Cohard, J., Hector, B., Lawin, E.A., Chagnaud, G., Danso, D.K., *et al.* (2023) Evaluation of Reanalysis Estimates of Precipitation, Radiation, and Temperature over Benin (West Africa). *Journal of Applied Meteorology and Climatology*, **62**, 1005-1022. https://doi.org/10.1175/jamc-d-21-0222.1

[25] Ouranos et Oxfam (2020) Atlas climatique du Bénin. Ouranos and Oxfam Quebec, Montréal.

[26] Vadrevu, K.P. and Choi, Y. (2011) Wavelet Analysis of Airborne CO_2 Measurements and Related Meteorological Parameters over Heterogeneous Landscapes. *Atmospheric Research*, **102**, 77-90. https://doi.org/10.1016/j.atmosres.2011.06.008

[27] Torrence, C. and Compo, G.P. (1998) A Practical Guide to Wavelet Analysis. *Bulletin of the American Meteorological Society*, **79**, 61-78. https://doi.org/10.1175/1520-0477(1998)079<0061:apgtwa>2.0.co;2

[28] Cazelles, B., Chavez, M., Berteaux, D., Ménard, F., Vik, J.O., Jenouvrier, S., *et al.* (2008) Wavelet Analysis of Ecological Time Series. *Oecologia*, **156**, 287-304.

https://doi.org/10.1007/s00442-008-0993-2

[29] Percival, D.B. and Walden, A.T. (2000) Wavelet Methods for Time Series Analysis. Cambridge University Press. https://doi.org/10.1017/cbo9780511841040

[30] Vargas, R., Detto, M., Baldocchi, D.D. and Allen, M.F. (2010) Multiscale Analysis of Temporal Variability of Soil CO_2 Production as Influenced by Weather and Vegetation. *Global Change Biology*, **16**, 1589-1605. https://doi.org/10.1111/j.1365-2486.2009.02111.x

[31] Kounouhéwa, B., Mamadou, O., N'Gobi, G.K. and Awanou, C.N. (2013) Dynamics and Diurnal Variations of Surface Radiation Budget over Agricultural Crops Located in Sudanian Climate. *Atmospheric and Climate Sciences*, **3**, 121-131. https://doi.org/10.4236/acs.2013.31014

[32] Danso, D.K., Anquetin, S., Diedhiou, A., Kouadio, K. and Kobea, A.T. (2020) Daytime Low-Level Clouds in West Africa—Occurrence, Associated Drivers, and Shortwave Radiation Attenuation. *Earth System Dynamics*, **11**, 1133-1152. https://doi.org/10.5194/esd-11-1133-2020

[33] Matthew, O.J., Ayoola, M.A., Ogolo, E.O. and Sunmonu, L.A. (2020) Impacts of Cloudiness on Near Surface Radiation and Temperature in Nigeria, West Africa. *SN Applied Sciences*, **2**, Article No. 2127. https://doi.org/10.1007/s42452-020-03961-y